Correlation effects in Cr–Zinc chalogenides

C. Tablero

Instituto de Energía Solar, Universidad Politécnica de Madrid, Ciudad Universitaria s/n, 28040 Madrid, Spain

A B S T R A C T

The electronic properties and self-interaction effects of $Zn_{1-x}Cr_xTe$ (with $x = 0.03125$ and 0.0625), using the local spin density Approximation with a Hubbard term to improve the description of the d-Cr orbitals, is presented. These materials have potential technological applications as half-metallic and intermediate band materials. For a sufficiently high density of Cr substituting the Zn atoms they have an intermediate band in the host semiconductor band gap for a one spin component, with the Fermi energy located within the impurity band. An increase in the Cr concentration causes an overlap of the intermediate band with the valence band, leading to only half-metallic behaviour. One would expect a substantial shift in the position of the Cr d-bands due to the local Coulomb interaction. However, the Coulomb interaction induces almost no changes in the occupied bands. The expected shift is indeed observed in the conduction band. This point is analyzed and a comparison with other zinc chalogenides is made in accordance with the interactions Cr-host semiconductor.

Keywords:
Self interaction
Intermediate band materials
Impurity band
Correlation
Solar cells
Spintronic
Lasers

1. Introduction

Cr-doped II–VI compound materials have been the subject of extensive research since the early 1960s. There is a large body of literature on these compounds as materials for light emission in the blue and green spectral regions. These materials have been of interest for their use in light emitting diodes, as well as blue lasers and fluorescent displays. These crystals have very recently attracted the attention of researchers as magnetic semiconductors for spintronics, transparent conducting oxides, up and down-converters and intermediate-band solar cells. Moreover, Cr can be incorporated into the wide-bandgap semiconductor, such as ZnS or ZnSe, and exhibit room-temperature operation in the mid-infrared.

For spintronic applications it is highly desirable to explore satisfactory half-metallic (HM) ferromagnetic materials compatible with traditional III–V and II–VI semiconductors. After the discovery of the ferromagnetism of $Ga_{0.947}Mn_{0.053}As$ with a high Curie temperature, the diluted magnetic semiconductors (DMS) became the subject of intensive experimental and theoretical studies as they were considered to be promising materials for semiconductor spintronics. Very recently a $Zn_{1-x}Cr_xTe$ sample with a high Cr concentration of $x = 0.20$ has been grown Therefore, it is of much interest to explore the electronic and magnetic properties and structural stability of ternary transition metal compounds based on ZnTe.

Interest in optoelectronics has now brought about the development of materials from semiconductors with high concentrations of levels within the semiconductor band gap, known as intermediate band materials (IBM) with three main characteristics. Firstly, these materials have an isolated intermediate band (IB) with respect to the valence band (VB) and the conduction band (CB) of the host semiconductor. If the IB overlaps and merges with the VB or the CB of the host semiconductor, the electron-phonon interaction will produce thermal relaxation as a result of the interaction between the electrons and the phonons coming from the lattice. These materials would therefore not be suitable for optoelectronic devices based on IBM. The second characteristic is that the IB should have a finite, but not excessive, width, so that it is isolated from the VB and the CB of the host semiconductor. Finally, the IB must be partially filled. Therefore, in a formal band-theoretic picture, the IB is metallic because the Fermi energy is located within the impurity band. This basic electronic band structure is a characteristic of transparent-conducting oxides, up- and down-converters, some mid-infrared lasers and intermediate-band solar cells. Note that this structure is a particular, though more restrictive, case of DMS, where the system has two band gaps and an IB

for a spin component. Therefore, if the IB for a spin component mixes with the host bands, the material will no longer be an IBM, although it will continue to be an HM material. Of course, also there are IBMs that are not HM materials, when the IB is present for the two spin components.

It is also important to note that the Cr-doped zinc chalogenides combine the properties of semiconductors with those of the traditionally used dielectric laser materials As a result, they possess the excellent laser properties along with interesting physics as well as optical and nonlinear properties, distinguishing them from the traditionally used dielectric laser media. This opens up an exciting wide field of research and new opportunities for the use of these materials in laser and nonlinear optical applications.

Several zinc chalogenides, $Zn_{1-x}Cr_xY$ with Y = S and Te, have been studied both theoretically and experimentally. the bulk systems $Zn_{1-x}Cr_xTe$ with x from 0.25 to 0.75 are analyzed theoretically. Samples with a high Cr concentration ($x = 0.2$) have also been grown These systems are characterized by a high Curie temperature and HM behaviour with only spin-up states present at the Fermi energy. The spin-up and spin-down impurity bands do not overlap, which leads to strong HM behaviour with only spin-up states present at the Fermi energy. For these x values, an isolated, partially filled IB is not seen. However, theoretical studies indicate the possibility of the presence of an IB for much smaller concentrations ($x = 1/32 = 0.03125$ and $1/108 = 0.00926$).

To date, the main body of theoretical studies has been carried out within the framework of the density functional theory (DFT) For instance, many DFT calculations for the III–V, II–VI DMS and IBM have been carried out with the local spin density approximation (LSDA) and generalized gradient correction (GGA) for the exchange and correlation term. However, the currently used exchange and correlation functionals are built from a homogeneous electron gas so that interactions are treated in a mean field approach which is not accurate enough to describe correlations properly or account for other many-body effects. The LSDA and GGA tend to underestimate the Coulomb repulsion of electrons occupying different orbitals of the same d shell. In particular, this leads to equal occupations of different orbitals of the same manifold and prevents stabilization of the orbitally-ordered solutions.

Because of the narrow and partially filled IB characteristics, the correlation effects should be very important. The IB electrons are supposed to spend their time in regions (around the ions) where the presence of other particles would make them feel strong Coulomb repulsion, thus making their motion correlated. The band structure LSDA calculations are not the best approach to observe this physical behaviour, because it is the manifestation of a single-particle problem, whereas the correlation is the result of many-body interactions. Because of the correlation effects, the IB could split into two sub-bands, a full one and an empty one. Therefore, a more profound study of these materials with respect to the correlation effect would be desirable to analyze whether this band overlaps with the VB, similar to what happens for larger concentrations. In this case, as has been previously mentioned, the material would be transformed from an IBM and HM material to just an HM material. The possible approaches [7] for this study are Green functions with screened interaction (GW), the self-interaction correction to the LSDA (LSDA-SIC), the Exact Exchange Kohn–Sham formalism (EXX), and to include in the LSDA a Hubbard term U to improve the description of the many-body effect (LSDA + U). The GW, SIC and EXX formalisms are currently prohibitively expensive for large cells. For an intermediate level, the LSDA + U method with a Hubbard term (U) greatly improves the description of the IB states and allows relatively larger supercells to be analyzed. Moreover, it generates an orbital-dependent potential which favours solutions with broken orbital degeneracy.

the bulk systems $Zn_{1-x}Cr_xY$ with Y = S and Se and $x \leqslant 0.0625$, with an IB for the majority spin component, are analyzed theoretically with the LSDA + U methodology for a wide range of U (from U = 0 to U = 6 eV). Nevertheless, the theoretical calculated values of U (overestimated) for these systems are around 2 eV.

for U > 6 eV, Y = S and $x = 1/32 = 0.03125$, a metal insulator transition takes place. for U = 6 eV, Y = S and $x = 2/32 = 0.0625$ this transition does not happen. However, for U > 6 eV, a splitting of the d_{xz}-Cr and the p_y-Cr orbitals produces two Hubbard sub-bands, a full one below the Fermi energy and an empty one above the Fermi energy. The metal-insulator transition does not happen because the other contributions to the IB are not separated by a gap, and therefore, the band is not split.
for Y = Se it is emphasized that the correlation effects when Cr substitutes Zn atoms in the ZnSe host semiconductor are lower than when the host semiconductor is ZnS.

Summarizing, the $Zn_{1-x}Cr_xTe$ with $x = 0.2$ has been grown and has been analyzed theoretically for $x > 0.2$ presenting HM behaviour with only spin-up states present at the Fermi energy. Theoretical studies, using the LSDA methodology , indicate the possibility of the presence of an IB for much smaller concentrations ($x \leqslant 1/32$). Therefore, it is desirable to extend the study of the $Zn_{1-x}Cr_xTe$ beyond the LSDA to analyze whether a smaller Cr concentration, as well as the HM behaviour, leading to the formation of a partially filled IB. Note that the overlapping of the IB with the VB has, as a consequence, the HM behaviour observed experimentally and theoretically for $x = 0.2$.

The present work is important in a number of aspects. We will analyze the theoretical results for $Zn_{1-x}Cr_xTe$ with $x = 1/32$ and $x = 2/32$ in order to check whether the IB mixes with the VB. Because of the DFT–LSDA limitations, a further extension beyond the LSDA is carried out using the LSDA + U method. The results of the LSDA + U method seem surprising due to the small influence of the U-parameter on the electronic properties of the IB. These results and the variation with the host semiconductor will be analyzed, and the differences discussed.

2. Calculations

The computation of total energies from first principles requires the finding of solutions to the Schrödinger equation using DFT [12]. Initially, we simplify the many-body electronic problem by making use of the DFT–LSDA. For the exchange and correlation term, the LSDA has been used as proposed by Ceperley–Alder A well-known consequence of using the LSDA is the fact that the band gap is usually underestimated. On the other hand, the use of the LSDA considerably simplifies the solution of the Schrödinger equation by mapping it into a single-electron equation. The electronic structure calculations were carried out by using pseudopotentials for core electrons. The standard Troullier–Martins pseudopotential is adopted and expressed in the Kleinman–Bylander factorization. The standard Kohn–Sham (KS) equations are solved self-consistently and the KS orbitals are represented by using a linear combination of confined numerically-localized pseudoatomic orbitals

An analysis of the basis set convergence has been carried out using from single-zeta to double-zeta with polarization basis sets for all atoms and varying the number of the special k points in the irreducible Brillouin zone (BZ). In all calculations a double-zeta with polarization functions basis set has been used. We use periodic boundary conditions with 18 special k points in the irreducible BZ for the 64-atom cell. For almost all calculations, the zinc blende ZnTe experimental lattice constant of 6.10 Å has been assumed. Nevertheless, in order to analyze whether a distortion splits the occupied and empty IB states, the Cr and nearest

neighbor cell-internal atom positions were allowed to relax in accordance with the calculated quantum mechanical forces until the forces became smaller than 0.004 eV/Å.

In the currently used exchange and correlation functionals, the interactions are handled in a mean field approach which is not suitable for describing correlation effects properly. One of the fundamental problems intrinsic to the LSDA is the presence of self-interaction. This is the spurious interaction of an electron in a given KS orbital with the Hartree and the exchange-correlation potential generated by itself. In order to remove the self-interaction, in LSDA + U one replace the LSDA exchange and correlation energy associate to the correlated orbitals with the Hubbard-U energy. Then, the LSDA + U method corrects the spurious self-interaction for the shells where it is applied, while the remaining ones are still affected by the self-interaction error. Therefore, in order to analyze the effect of the self-interaction in the IB, a further extension beyond the LSDA is carried out using the LSDA + U method, including an orbital-dependent one-electron potential to account explicitly for the important Coulomb repulsions not adequately handled in the LSDA approach. Several forms and implementations have proposed to date The LSDA + U method used here has been applied to similar systems using the same calculation methodology A weakness of the LSDA + U method is that U is an external parameter. The screened U parameter has been estimated theoretically using constrained LSDA calculations by varying the occupation numbers of the *d* orbitals. The value obtained gives U ~ 2.0 eV. However, in many cases the value of U obtained theoretically is different from the optimal value determined empirically as a fitting parameter to experimental results. Therefore, this theoretical value must be considered as an approximate value. Therefore, we present the results as a function of U and will argue that the correct physics is obtained within the interval 0 < U < 6 eV analyzed in this work.

3. Results

Using the methods described above, we have explored the $Zn_{1-x}Cr_xTe$, based on the zinc blende ZnTe host semiconductor, where x takes values of 1/32 and 2/32 to simulate heavy doping. The doping of $x = 1/32$ (2/32) is obtained by replacing the Zn by Cr at the apex and/or face-centre sites of the unit cell of zinc blende ZnTe with 64 atoms. For the host semiconductor, the Zn site is tetrahedrally surrounded by four equivalent Te atoms. However, when a Zn atom is substituted by Cr the Te atoms can be broken down into two groups: those directly bonded to the Cr atoms (Te_1) and those which are not (Te_2). Therefore, the Cr atoms will interact mainly with the Te_1 atoms. In these structures the antiferromagnetic alignment is less stable than the ferromagnetic (around 0.11 eV per cell for $x = 2/32$). It is in agreement with the literature Therefore we will focus our study on the ferromagnetic alignment.

The energy-band diagram in the principal directions of the BZ is shown in Fig. 1 with U = 0 eV. First of all, we see the HM behaviour in the sense that at the Fermi energy the density of states is finite for the majority spin and zero for the minority spin. For the minority spin components (—) there is a gap, similar to that of the host semiconductor. Moreover, an isolated IB for the majority spin component, made up of a group of three and six sub bands for $x = 1/32$ (Fig. 1a) and $x = 2/32$ (Fig. 1b) respectively, appears between the full band (VB) and the empty band (CB). The Fermi energy (horizontal line in the figure) cuts this IB showing that the band is partially filled. The IB for $x = 2/32$ has a bandwidth greater than $x = 1/32$ because of the larger concentration of Cr atoms.

When the positions of the Cr and of its nearest neighbors are relaxed (according to the calculated quantum mechanical forces until the forces became smaller than 0.004 eV/Å), the distances Cr–Te

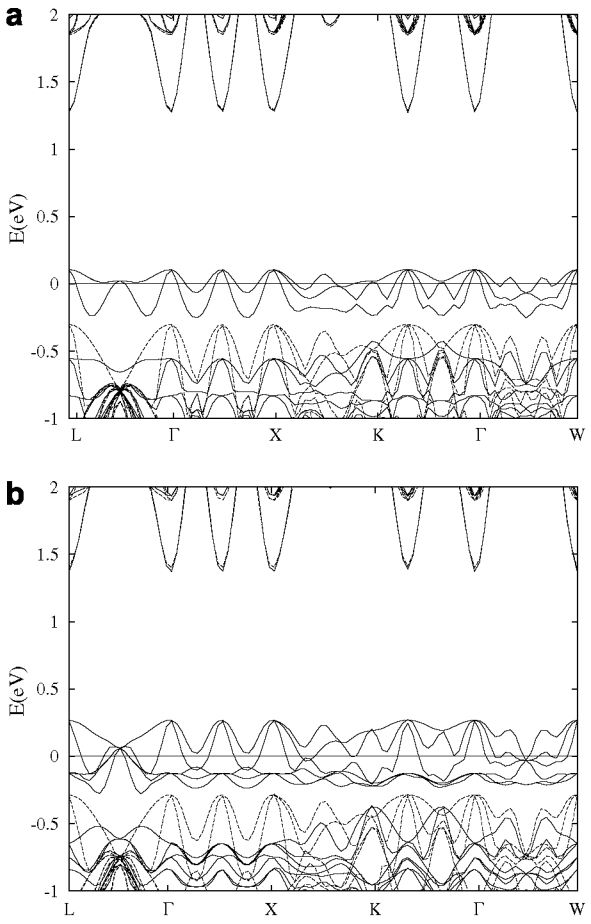

Fig. 1. Energy bands (eV) in the principal directions of the Brillouin zone for $Zn_{1-x}Cr_xTe$ with (a) $x = 1/32$ and (b) $x = 2/32$, for the majority (solid lines) and minority spin component (dotted lines). The Fermi energy as zero has been chosen in this figure.

increase with respect to the distances Zn–Te of the host semiconductor (2.64 Å) and the local tetrahedral symmetry (considering the immediate Cr neighbors) is reduced to C_{3v}: there are three same distances (2.78 Å) and a different one (2.69 Å). The Cr-neighbors suffer an outward non-symmetrical displacement. Moreover, the relaxing of the atomic positions causes a downward shift of the IB with respect to the VB. Nevertheless, this distortion does not produce a split of the occupied and the empty IB states.

In order to identify the atomic and orbital composition of these bands, the projected density of states (DOS) of the atoms and Cr orbitals is represented in Fig. 2. For all concentrations, it can be seen that the IB is created for combination of the Cr and Te_1 orbitals (direct bonding to the Cr atoms). From the figure, it can also be seen that the Cr orbitals that contribute more to the IB are the d orbitals with t symmetry (d_{xy}, d_{xz} and d_{yz}), and in a lower proportion, the p orbitals (also of t symmetry). Although both, the d_{xy}, d_{xz} and d_{yz} (t–d Cr orbitals) and p–Cr orbitals have t symmetry, we will refer from now on to the t–d Cr orbitals and e–d Cr orbitals (d_{z^2} and $d_{x^2-y^2}$) as t–Cr and e–Cr orbitals. Note that in Fig. 2 the projected DOS on atoms are per atom. It doesn't include the sum on all the atoms. There are 4 and 8 Te_1 atoms for $x = 1/32$ and 2/32 in the 64-atom supercell. Therefore, the total DOS corresponding to all Te_1 atoms is 4 and 8 times larger respectively than in Fig. 2a and c. The percentages of Cr atom in the IB with respect to Te_1 atom are, at least, 4 or 8 times smaller than in these figures respectively.

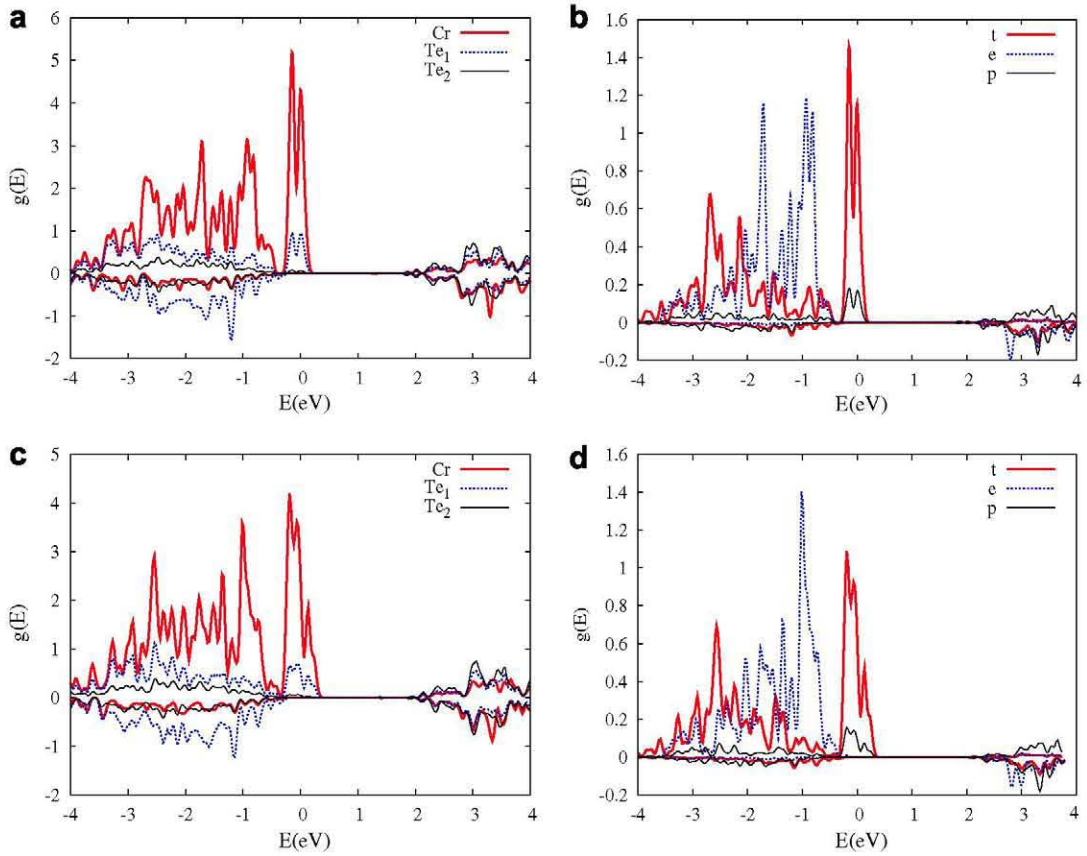

Fig. 2. Projected DOS for the $Zn_{1-x}Cr_xTe$ systems on the Te and Cr atoms (per atom, with $x = 1/32$ (a) and with $x = 2/32$ (c)), and the d (t and e) and the p Cr orbitals ((b) with $x = 1/32$ and (d) with $x = 2/32$). The Fermi energy as zero has been chosen in this figure.

The total integrated DOS between the bottom of the IB and the Fermi energy is two and four electrons per cell for $x = 1/32$ and $x = 2/32$, respectively, and between the Fermi energy and the top of the IB is one and two electrons per cell for $x = 1/32$ and $x = 2/32$. This confirms the partial occupation of the IB. An analysis in a wider range of energy indicates that the t_-–Cr orbitals (t–Cr orbitals for minority spin component) contribute mainly to the VB, and the t_+–Cr orbitals (t–Cr orbitals for majority spin component) to the VB and IB. Therefore, the t–Cr orbitals mix with the t–Te_1 orbitals, forming a bonding component in the VB and an anti-bonding component in the IB for the majority spin component. This point will be discussed later.

For computational ease, in LSDA calculations with partially filled bands the one-particle charge density belongs to the totally symmetric representation of the physical symmetry group. For this, the contribution of the three t–Cr orbitals is equal. The same effect happens with the two e–Cr and three p–Cr orbitals. This symmetrization deprives a part of spatial correlation to the system allowing, for example, a different orbital occupation to minimize the effects of the Coulomb self-repulsions. LSDA + U methodology, with orbital-dependent potential, favours solutions with broken orbital degeneracy, i.e. a different spatial occupation. This fact can be seen in Figs. 3 and 4 for $x = 1/32$ and $x = 2/32$, and U = 3 and 6 eV.

In these figures, the t–Cr, the e–Cr and the p–Cr orbitals are split into several components. The three t–Cr orbitals are divided into two groups, one made up of the d_{xy} orbital and the other one of the d_{xz} and the d_{yz} orbitals. The e–Cr orbital group is separated in its components. The three p–Cr orbitals are divided into two groups, one formed by the p_z orbital and the other one by the p_x and the p_y orbitals. However, these separations are small, indicating that the U effect does not significantly affect the IB. This fact also can be seen in Tables 1 and 2.

In Table 1 the gaps and bandwidths for U = 0, 3 and 6 eV are shown. For the majority spin component (+), $\Delta E_{VI}^{(+)}$, $\Delta E_{I}^{(+)}$ and $\Delta E_{IC}^{(+)}$ are the gap between the VB maximum and the IB minimum, the IB bandwidth (the difference between the IB maximum and IB minimum), and the gap between the IB maximum and the CB minimum. Similarly, $\Delta E_{VC}^{(-)}$ is the gap between the VB maximum and the CB minimum for the minority spin component. As U increases from 0 to 6 eV, the variation in these magnitudes is small, indicating, as mentioned, the small influence of the U-Hubbard term. The gaps $\Delta E_{VC}^{(-)}$ and $\Delta E_{VC}^{(+)}$ ($\Delta E_{VI}^{(+)} + \Delta E_{I}^{(+)} + \Delta E_{IC}^{(+)}$) in our calculations are about half of the value known from experiments of the host semiconductor (2.3 eV). The calculated gap with the same 64-cell atoms of the host semiconductor and equal conditions is 1.50 eV. Comparing this value with those of Table 1, the introduction of Cr increases the band gap slightly with respect to the host semiconductor. This gap dependence on the Cr concentration is similar to other results with more Cr concentration [5]. Nevertheless, it is necessary to point out that the LSDA underestimates the gaps and that LSDA + U method does not correct the spurious self-interaction for the host semiconductor.

The small U effect also can be seen in Table 2, where the population analysis of the Cr atom and of the Cr orbitals is show. The U effect is so small that the different components seen in the projected DOS have the same population analysis for the precision shown in the Table. For this reason these components are grouped into the original t, e and p-Cr components. For the two concentrations the results are similar. It is interesting to note that the total charge of the Cr atom is smaller than the six valence electrons. It means that the Cr orbitals mix with the host orbitals. Moreover,

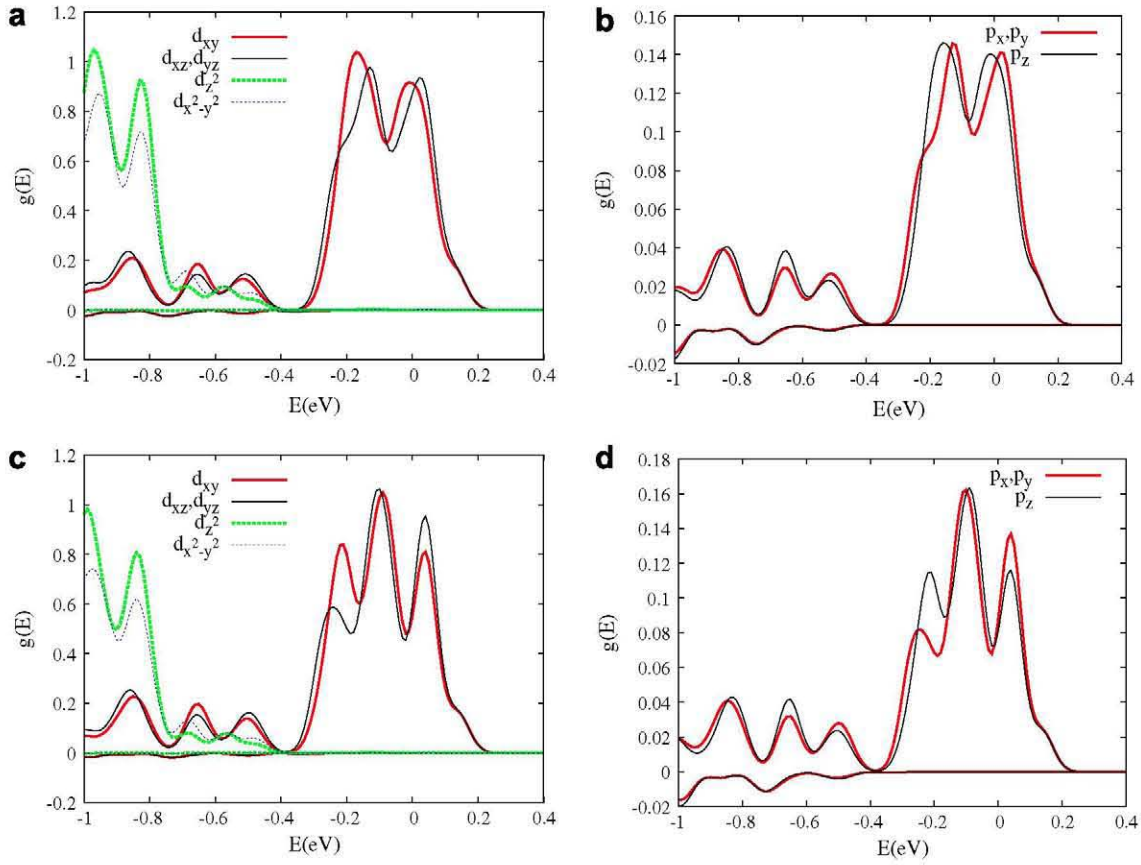

Fig. 3. Projected DOS for the $Zn_{1-x}Cr_xTe$ with $x = 1/32$ on: (a) d-Cr orbitals with U = 3 eV; (b) p-Cr orbitals with U = 3 eV; (c) d-Cr orbitals with U = 6 eV; (d) *p*-Cr orbitals with U = 6 eV. The Fermi energy as zero has been chosen in this figure.

the difference between the two spin components, proportional to the atomic polarization, increases with U.

As an important conclusion, the results indicate that the correlation effects are not very important compared with other semiconductors . These ternary compounds, and others based on III–V and II–VI host semiconductors could have applications in the near future, as HM materials, or IBM for lower concentrations, especially those with $x < 1/32$. As HM materials, quite high Curie temperatures would be expected in many of them because of their quite wide HM gaps

4. Discussion

4.1. Comparison with others zinc chalogenides

Zinc chalogenides $Zn_{1-x}Cr_xY$ with Y = S and Se and with $x = 1/32$ and $x = 2/32$ (and to $x = 108$ using only LSDA) have been studied using the same methodology as for Y = Te in this work. Firstly, the main conclusions of these works will be summarized, and later on we will carry out a comparative analysis of the Cr doped zinc chalogenides.

The correlation effects of the $Zn_{1-x}Cr_xS$ are analyzed for U > 6 eV and with $x = 1/32$, a metal insulator transition takes place. for U = 6 eV and $x = 2/32$ the IB is not split, although for U > 6 eV, the d_{xz} and p_y components for the majority spin component are split from the t-Cr and p-Cr orbitals. This fact results from an increase in the Cr concentration which produces an increase in the width of the IB, and the correlation effects diminish. For the $Zn_{1-x}Cr_xSe$ analyzed in Ref. [11], no splitting of the IB is seen and the correlation effects are lower than for $Zn_{1-x}Cr_xS$.

The values estimated theoretically of the screened U for these systems, using constrained LSDA calculations by varying the occupation numbers of the d orbitals, are around 2 eV. The results obtained for $Zn_{1-x}Cr_xSe$ with $x = 1/32$ using total energy calculations in different charge states and atomic positions as difference between donor and acceptor levels is ~1.3 eV, in good agreement with the results of the literature (~1.5 eV).

The results for $Zn_{1-x}Cr_xTe$, and the other results for $Zn_{1-x}Cr_xY$ with Y = S and Se, mean that the variations in the characteristics of the VB and IB with U are very small. The contribution to the projected DOS with U of the Cr-d bands (Figs. 2–4) remains largely intact and the changes in orbital occupancies are fairly small. The LSDA + U method usually favours the complete occupancy of certain orbitals, while empty ones are shifted upwards in energy. However, in the present case, the d-bands of the Cr atom remain uniformly occupied. Of course, there are slight variations between the t, e and p-Cr orbitals because the LSDA + U include a spatial correlation degree associated with the anisotropy in the occupation numbers.

The Coulomb interaction induces almost no changes in the occupied bands (the full VB and the partially filled IB). One would expect a substantial shift in the position of the empty Cr d-bands in LSDA + U due to the local Coulomb interaction U. This expected shift of the Cr d-bands is indeed seen in the CB. It is due to the interactions between the Cr and the host.

This can be analyzed using a simple model, considering the host and impurity states without interaction ($\varphi_H^{(0)}$ and $\varphi_I^{(0)}$), separated for an energy $\Delta^{(0)}$, and coupled for the matrix element *V*. When the interaction takes place, the initial states mix, giving rise to the new states $\varphi_H^{(\theta)} = \cos\theta \cdot \varphi_H^{(0)} - \sin\theta \cdot \varphi_I^{(0)}$ and $\varphi_I^{(\theta)} = \sin\theta \cdot \varphi_H^{(0)} + \cos\theta \cdot \varphi_I^{(0)}$, separated for an energy $\Delta^{(\theta)} = \Delta^{(0)}$ sec 2θ, where

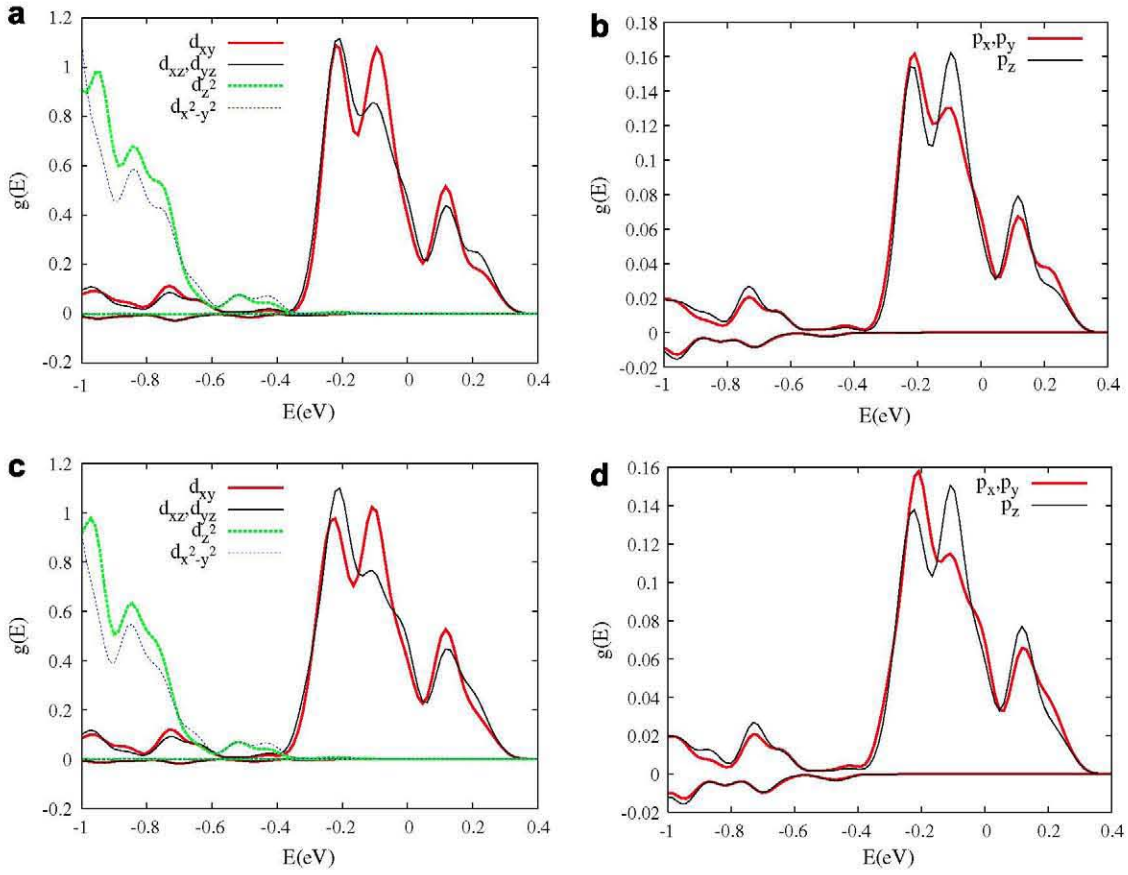

Fig. 4. Same legend as Fig. 3 with $x = 2/32$.

Table 1
Energies (eV) of the $Zn_{1-x}Cr_xTe$ systems for several x and U (eV) values

x	U	$\Delta E_{VI}^{(+)}$	$\Delta E_{I}^{(+)}$	$\Delta E_{IC}^{(+)}$	$\Delta E_{VC}^{(-)}$
1/32	0	0.17	0.36	1.16	1.58
1/32	3	0.24	0.37	1.16	1.57
1/32	6	0.21	0.41	1.16	1.56
2/32	0	0.19	0.52	1.10	1.68
2/32	3	0.16	0.53	1.11	1.66
2/32	6	0.13	0.55	1.12	1.64
1/32[a]	0	0.24	0.31	1.22	1.56

$\Delta E_{VI}^{(+)}$, $\Delta E_{IC}^{(+)}$ and $\Delta E_{I}^{(+)}$ are the VB-IB gap, the IB-CB gap and the IB width for the majority spin component. $\Delta E_{VC}^{(-)}$ is the VB-CB gap for the minority spin component.
[a] With the atomic positions relaxed.

Table 2
Mulliken population analysis of the Cr atoms and the Cr orbitals

x	U	q_+/q_-	t_+/t_-	e_+/e_-	p_+/p_-
1/32	0	5.48/0.91	0.86/0.05	0.96/0.01	0.17/0.11
1/32	3	5.50/0.87	0.86/0.04	0.97/0.01	0.18/0.11
1/32	6	5.51/0.85	0.86/0.02	0.97/0.01	0.18/0.12
2/32	0	5.49/0.91	0.86/0.05	0.96/0.01	0.17/0.11
2/32	3	5.50/0.87	0.86/0.03	0.97/0.01	0.18/0.11
2/32	6	5.51/0.85	0.90/0.02	0.97/0.01	0.18/0.12
1/32[a]	0	5.48/0.88	0.86/0.05	0.96/0.01	0.17/0.11

The spin component is shown in subscript: (+) for majority and (−) for minority spin respectively. In the table $q_\pm$ is the total atomic charge.
[a] With the atomic positions relaxed.

$\tan 2\theta = 2V/\Delta^{(0)}$. If initially the occupation number of the $\varphi_I^{(0)}$ state without interaction is $n_I^{(0)}$, the occupation numbers of the state $\varphi_I^{(\theta)}$ and $\varphi_{II}^{(\theta)}$ are $n_I^{(\theta)} = n_I^{(0)} \cos^2\theta$ and $n_{II}^{(\theta)} = n_I^{(0)} \sin^2\theta$. Therefore, as is well known, the states are repelled when increasing the interaction, moving the one with smaller energy to lower energy and the one with higher energy to larger energy, thus increasing their energetic separation $\Delta^{(\theta)}$. Moreover, the resulting states after of the combination reduce the character (contribution) of the initial energy nearest state. The $\varphi_I^{(\theta)}$ and $\varphi_{II}^{(\theta)}$ states have anti-bonding (larger energy) and bonding (smaller energy) character, respectively. From this simple model we can obtain significant consequences. For example, it explains the small effective $U^{(\theta)}$ in the solid, because the atomic $U^{(0)}$ value is renormalized in the solid as a consequence of the interaction. The Mott–Hubbard Coulomb repulsion in the $\varphi_I^{(\theta)}$ is $E \sim (U^{(0)}/2)[n_I^{(\theta)}]^2 = (U^{(\theta)}/2)[n_I^{(0)}]^2$, where $U^{(\theta)}/U^{(0)} = \cos^4\theta < 1$. Therefore, an increase in the interaction produces a reduction in the effective Coulomb repulsion. This is why the $Zn_{1-x}Cr_xY$ with Y = S, Se, and Te the Cr-d bands remain largely intact and the changes in orbital occupancies are fairly small with an increase in U.

An analysis of the DOS for the d-Cr orbitals in a larger range of energy that of the previous figures indicates that the t_+ spin up component contributes principally to the VB and to the IB, the e_+ spin up component contribute principally to the VB, and the t_- and the e_- spin down components contribute principally to the CB. The bonding orbital t_+-Cr in the VB has an anti-bonding counterpart in the IB, whereas the e_+-Cr bonding and anti-bonding combinations are into of the VB. Because of the strong interactions with the host orbitals, the t-Cr and e-Cr orbitals in the VB are affected little for U, and the t_+-Cr of the IB are slightly affected. As has been previously mentioned, the expected shift in the Cr d-bands is indeed seen in the CB on the t_--Cr and the e_--Cr orbitals, where these orbitals experience a displacement toward more energy with the increase in U. It is due to the small combination with the host orbitals.

From another point of view, this can be explained using directly the LSDA + U methodology. From the LSDA + U, the energy of a monoelectronic level is $\varepsilon^{(\sigma)}_{m\,[\mathrm{LSDA+U}]} = \varepsilon^{(\sigma)}_{\mathrm{m}\,[\mathrm{LSDA}]} + U^{(\sigma)}_{\mathrm{m}}(1/2 - n^{(\sigma)}_{\mathrm{m}})$, where $n^{(\sigma)}_{\mathrm{m}}$ are the elements of the occupation number matrix for spin σ of the m orbital, which is calculated self-consistently within this approach. Therefore, the occupied and unoccupied orbitals are shifted by $-U^{(\sigma)}_{\mathrm{m}}/2(n^{(\sigma)}_{\mathrm{m}} = 1)$ and $U^{(\sigma)}_{\mathrm{m}}/2(n^{(\sigma)}_{\mathrm{m}} = 0)$, respectively, reproducing the correct physics of a Mott–Hubbard transition qualitatively. Nevertheless, regarding this qualitatively interpretation some aspects must be pointed out. The key to the understanding lies in $n^{(\sigma)}_{\mathrm{m}}$, the elements of the occupation number of the m orbital matrix. It should not be it confused with the occupation of the bands. They are two different things. If a band is only formed by the m orbital, the previous qualitative reasoning is correct. However, if the contribution of the m orbital to the band is very small, then the split is also very small, or equivalently, the effective U is reduced by combination of the m orbital with the host-semiconductor. It explains the small shift in the IB because of the combination of the t-Cr orbitals with the anion Y-orbitals. Moreover, as the t_+ and e_+ spin up components contribute principally to the VB and the spin down components contribute principally to the CB, the majority components experience a downward shift in the VB and the minority components and upward shift in the CB. These shifts are low in the VB because of the larger combination of the Cr-Y orbitals.

As we move to lighter impurities (Y), the orbitals of the impurity atom become closer to those of the t-host states. The availability of host states of the same symmetries and compatible energies then leads to the formation of a broad t contribution to the VB (i.e., t–d of the Cr atom and t(p)-host bonding combination). This interaction leads to a stronger repulsion of the anti-bonding combination and to the appearance of a band (i.e. the IB) in the gap. Therefore, as the interaction increases, an IB can arise in the gap with lower proportion of d-Cr character and lower effective U. An analysis of the DOS confirm that the contribution of the t_+-Cr to the IB is larger for the S and smaller for Te. Accordingly, when Y = Te, the IB has more energy (it is more strongly repelled by the VB) and lower effective U because of the larger interaction with the host, with respect to Y = S and Se atoms. However, there is another effect opposite to the previous one: the energy of the VB increases as we move to lighter impurities. To achieve this, the IB overlaps with the VB for Y = Te, although the interaction between the host and impurity orbitals is larger (lower proportion of d-Cr character into the IB).

5. Conclusions

Summarizing, the electronic properties of $Zn_{1-x}Cr_xTe$ with $x = 1/32$ and $2/32$ have been studied. This alloy is HM and it has been grown for $x = 0.2$. These compounds present an IB for majority spin component and for $x < 1/32$. For a larger concentration the IB mixes with the VB, resulting in the HM behaviour. The electronic properties when LSDA + U methodology is used present slight variations with respect to LSDA. The broken orbital-occupation degeneracy is almost not observed.

The shift in the position and splitting of the partially filled IB because of the local Coulomb interaction U is very small. The Coulomb interaction induces almost no changes in the occupied bands (the full VB and the partially filled IB). The expected shift in the Cr d-bands is indeed observed in the CB. It is caused by the interactions between the Cr and the host. The interactions between the Cr and host orbitals of the zinc chalogenides are analyzed, showing that the U effect decreases from S to Te. Moreover, these interactions are responsible for the effective decrease in the value of U.

References

H. Ohno, A. Shen, F. Matsukura, A. Oiwa, A. Endo, S. Kutsumoto, Y. Iye, Appl. Phys. Lett. 69 (1996) 363.
H. Saito, V. Zayets, S. Yanagata, K. Ando, Phys. Rev. Lett. 90 (2003) 207202.
A. Luque, A. Martí, Phys. Rev. Lett. 78 (1997) 5014;
A. Luque, A. Martí, Prog. Photov, Res. Appl. 9 (2) (2001) 73;
A. Martí, L. Cuadra, A. Luque, in: Proceedings of the 28th IEEE Photovoltaics Specialists Conference, 940, New York: IEEE, 2000;
K.M. Yu, W. Walukiewicz, J. Wu, W. Shan, J.W. Beeman, iM.A. Scarpulla, O.D. Dubon, P. Becla, Phys. Rev. Lett. 91 (24) (2003) 246403–246411.
L.D. DeLoach, R.H. Page, G.D. Wilke, S.A. Payne, W.F. Krupke, IEEE J. Quantum Electron. 32 (1996) 885;
V.A. Kasiyan, R.Z. Shneck, Z.M. Dashevsky, S.R. Rotman, Phys. Status Solidi 229 (2002) 395.
L.M. Sandratskii, P. Bruno, J. Phys.: Condens. Matter 15 (2003) L585;
Q. Wang, Q. Sun, P. Jena, Y. Kawazoe, J. Appl. Phys. 97 (2005) 043904;
Wen-Hui Xie, Bang-Gui. Liu, J. Appl. Phys. 96 (2004) 3559.
C. Tablero, Sol. Energy Mat. Sol. C 90 (2006) 588;
C. Tablero, Comput. Mater. Sci. 37 (2006) 483.
R.M. Martin, Electronic Structure, Basis Theory and Practical Methods, Cambridge University Press, 2004;
K. Ohno, K. Esfarjani, Y. Kawazoe, Computational Materials Science, From ab initio to Monte Carlo Methods, Springer, 1999;
R.G. Parr, W. Yang, Density Functional Theory of Atoms and Molecules, Oxford, New York, 1989;
J.F. Dobson, G. Vignale, M.P. Das, Electron Density Functional Theory, Recent Progress and New Directions, Plenum Press, New York, 1998.
C. Tablero, Solid State Commun. 133 (2005) 97–101;
C. Tablero, Phys. Rev. B 72 (2005) 035213–035221;
C. Tablero, Sol. Energy Mat. Sol. 90 (2006) 203;
C. Tablero, Sol. Energy Mat. Sol. C 90 (2006) 1734.
C. Tablero, J. Chem. Phys. 123 (2005) 114709.
C. Tablero, Phys. Rev. B 74 (2006) 195203.
C. Tablero, J. Chem. Phys. 126 (2007) 164703–164707.
P. Hohenberg, W. Kohn, Phys. Rev. 136 (1964) B864.
D.M. Ceperley, B.J. Alder, Phys. Rev. Lett. 45 (1980) 566.
N. Troullier, J.L. Martins, Phys. Rev. B 43 (1991) 1993.
L. Kleinman, D.M. Bylander, Phys. Rev. Lett. 48 (1982) 1425;
D.M. Bylander, L. Kleinman, Phys. Rev. B 41 (1990) 907.
W. Kohn, L.J. Sham, Phys. Rev. 140 (1965) A1133.
SIESTA code: J.M. Soler, E. Artacho, J.D. Gale, A. García, J. Junquera, P. Ordejon, D. Sánchez-Portal, J. Phys. Condens. Matter 14, 2002, 2745 and references therein.
O.F. Sankey, D.J. Niklewski, Phys. Rev. B 40 (1989) 3979.
V. I Anisimov, F. Aryasetiawan, A.I. Lichtenstein, J. Phys: Condens. Matter 9 (1997) 767;
A.I. Lichtenstein, V.I. Anisimov, J. Zaanen, Phys. Rev. B 52 (1995) R5467;
S.L. Dudarev, G.A. Botton, S.Y. Savrasov, C.J. Humphreys, A.P. Sutton, Phys. Rev. B 57 (1998) 1505.
The used code is a private modification of SIESTA code [17] where the author has implemented the DFT+U method. Details of this implementation can be found in the Ref. [11].
J. Kübler, Phys. Rev. B 67 (2003) 220403–220411.
C. Tablero, Solid State Commun. 143 (2007) 399.
M. Godlewski, M. Kaminska, J. Phys. C: Solid State Phys. 13 (1980) 6537;
V.A. Kasiyan, R.Z. Shneck, Z.M. Dashevsky, S.R. Rotman, Phys. Status Solidi 229 (2002) 395;
C.I. Rablau, J.O. Ndap, X. Ma, A. Burger, N.C. Giles, J. Electron. Mater. 28 (1999) 678;
G. Grebe, G. Roussos, H.J. Schulz, J. Phys. C 9 (1976) 4511;
S. Bhaskar, P.S. Dobal, B.K. Rai, R.S. Katiyar, H.D. Bist, J.-O. Ndap, A. Burger, J. Appl. Phys. 85 (1999) 439.